Optimized cluster centroids for segmentation of skin cancer using triangular intuitionistic fuzzy sets

Anupama **Namburu**[1], Senthilkumar **Mohan**[2], Sibi Chakkaravarthy[3] and Prabha Selvaraj[4]

[1]*School of Computer Science Engineering), VIT-AP University, Amaravathi, Guntur, India*

[2]*School of Computer Science Engineering, VIT, Vellore, India*

[3]*School of Computer Science Engineering), VIT-AP University, Amaravathi, Guntur, India*

[4]*School of Computer Science Engineering), VIT-AP University, Amaravathi, Guntur, India*

Abstract

Malignant Melanoma is a dangerous skin cancer and its detection is a challenging task as it appears in numerous ranges of size, shape, shading with various skin tones. Also, artifacts like hairs, outlines, blood vessels, and boils add further complexity. In this paper, a simplified clustering method is proposed to improve melanoma detection with reduced time complexity. The triangular membership function(TMF) is used to detect the initial regions for obtaining initial centroids. These initial centroids are used to apply intuitionistic fuzzy c-means clustering. The TMF helps in identifying the initial clusters and regions and reduces the number of iterations needed for segmentation. The proposed method effectively detects skin cancer regions with an average accuracy of 90% and performs well.

Keywords

LaTeX Fuzzy sets, intuitionistic fuzzy sets, medical image segmentation, image processing, skin cancer

1. Introduction

One of the most prevalent forms of cancer throughout the world is skin cancer and as per World Health Organization. It ranks 19th both in men and women with 324,635 cases reported in the year 2020. With the increased cases, the early detection and timely treatment for melanoma are critical for patient survival.

Dermoscopy is a well-known in vivo non-obtrusive imaging instrument that utilizes captivated light to help dermatologists in inspecting pigmented skin sores dependent on a lot of morphological highlights. In spite of the fact that dermoscopy has been appeared to prompt expanded demonstrative exactness, appropriate understanding of dermoscopic images is typically tedious, complex, costlier, and depends on the observer's perception. The traditional approaches are carried out with low-quality image processing methods which fall in image analysis in the medical field. The initial methods carried out in cleaning the raw data are done by pre-processing methods that adjust the intensity, contract, redundant data, scaling, and binarisation in the morphological structure of the image.

CEUR Workshop Proceedings (CEUR-WS.org)

The recent advancement in information technology is tremendous in showing high-performance results in detecting and diagnosing the different types of cancer, particularly skin cancer. The unwanted noises are removed pre-processing methods proposed by [1]. The quality of the image is enhanced by pre-processing methods which would reduce the processing time and time complexity.

Image resizing plays an important role while processing the data. As different datasets have varied sizes of images, it is necessary to resize them to the same size to apply the algorithms. The pre-processing is succeeded by Image segmentation to detect the region of interest (ROI). The ROI may be anything that we need to analyze. In the medical image, ROI could be the diseased region that is separated by the unaffected region [2]. This segments the unaffected tissue and then the required features are considered from the affected region so that the result will be accurate and clear [3].

The classical way of segmenting is performed by thresholding, clustering, and other edge detection methods, and the ABCDE method is used to diagnose melanoma in the skin during the analysis [4]. Even though many methods are incorporated in detecting and diagnosing cancer, there are still many challenges being faced while dealing with real-time image data. It contained many unpredicted complex data while the ocular emergence of the image in the affected skin area and causes difficulty in separating the desired ROI of melanoma with accurate contour measure from the image [5].

Automated state-of-the-art techniques have been developed to help dermatologists in improving their effectiveness and objectivity of visual understanding of dermoscopic images[6]. Automatic image segmentation is performed mainly using classification and clustering. Classification is supervised segmentation that requires prior information about the classes for classifying. Clustering is preferred as it is unsupervised and does not require prior information. However, clustering algorithms require initial centroids in order to obtain the clusters. Wrongly chosen clusters can result in local minima producing invalid segmentation regions, deeming the effort unfruitful.

Many researchers proposed automated methods to break these challenges. The broad category of these methods includes thresholding, clustering, classification, and contours & snakes, each having its merits and demerits [7].

Skin lesion segmentation based on thresholding namely, Otsu's[8], fuzzy logic [9], adaptive thresholding [10] are available in literature. The threshold methods lead to irregular edges with varied thresholds.

The lesions of a melanoma tend to have fuzzy borders and irregular shapes leading to uncertainty in identifying the exact lesion from skin images. Researchers have used fuzzy sets and rough sets to address the uncertainty and vagueness in the image. Skin cancer with fuzzy logic approaches are proposed in [11, 12, 13, 14]. Fuzzy-based methods have the advantage of representing the intermediate data in intervals allowing qualitative analysis of data [1]. A fuzzy intensity threshold with type2 fuzzy logic proposed in [9] was able to detect the pixel intensity either belongs to ROI or the background. These fuzzy-based methods failed to group lesion pixels with low contrast as lesions.

Garcia *et al.* use fuzzy classification of pixels and histogram threshold with innovative methods applied on skin images for segmentation in [15]. The method used otsu's threshold method and then fuzzified the regions and applied morphological operators to extract the

tissues in case of artifacts. Castillejos et al.[12] presented predefined cluster selection using fuzzy c-means. This work specifies automatically, the number of clusters needed by an image for segmentation. The clustering algorithms are highly influenced by the initial centroids and the number of clusters needed for clustering.

Many algorithms based on active contours and snakes are proposed for skin lesion segmentation [16, 17, 18, 19, 20, 21]. These algorithms usually depend on the initial curves and positioning of curves that undergo deformation to detect the boundaries of lesions. An automated method for adapting the contour to skin lesions is proposed in [21], but still, the contour selection is needed.

In recent days, many deep learning models for segmenting skin lesions are proposed in the literature using convolutional neural networks, generative adversarial models, deep autoencoders, stacked autoencoders, convolutional autoencoders, restricted Boltzmann's machine, and recurrent neural nets are reviewed and analyzed in [22, 23, 24, 25, 26]. Deep learning methods have the ability to obtain the features from images that are useful in segmentation. The performance of the deep learning models has improved when compared to existing methods. However, Graphics Processing Units (GPU) are used in parallel to analyze the features and to detect the skin lesions[6, 27, 28].

Adrian *et al.* use the trapezoidal intuitionistic fuzzy method for transferring the data into interval-valued trapezoidal multi-criteria for decision-making [29].In order to efficiently handle the data, intuitionistic fuzzy sets(IFS) provide a triple vector to make appropriate decision making. Aribarg has introduced a modified fuzzy ant-miner (MFAM) that employs attributes and case weighting for training in [30]. IFS was successfully applied for brain image segmentation for classifying tissues and tumors in presence of noise and artifacts [31, 32]. This motivated to use of IFS for segmenting skin lesions in presence of artifacts.

Intuitionistic fuzzy set(IFS) theory with medical images has been proposed to handle images with a lot of uncertainties, as they are badly illumined with fuzzy. Direct segmentation of results often creates unusable results. In [33] Charia *et al.* use IFS theory to produce accurate diagnosing of diseases using cellular images. FCM clustering method has been proposed by Huang *et al.* in [34] for image segmentation with rough set theory. The segmentation results of various clustering numbers under FCM where the image is distributed into various small regions based on the indistinguishable attributes with their relationship, have reduced error rates and improved segmentation of fuzzy boundary regions.

Advanced fuzzy set-theoretic techniques are very important and play a major role in the area of medical images. Digital pathology images with the IFS method are applied for segmentation of images. This method results in strong results compared to other segmentation methods [35, 36]. Shaw *et al.* show that triangular intuitionistic fuzzy numbers with arithmetic procedures can be used to check the reliability of the fuzzy systems. To calculate imprecise failure, each component failure is taken into considerations by the triangular intuitionistic fuzzy numbers [37][38].

Tilson *et al.* use FCM clustering programs for data analysis problems, and we have seen this method generate fuzzy classification for any set of given numerical data. The clustering method used to group the subsets and generalized objective with least square method [39]is proposed. Intuitionistic fuzzy c-means(IFCM) algorithm has been proposed for image segmentation in [40] for Brian images. Verma *et al.* use IFCM to handle the uncertainty. However, the results show that the method is very sensitive to noise and does not incorporate any local spatial information.

From this, ııғсм (improved intuitionistic fuzzy c-means) has been proposed to handle the insensitive to noise and freedom of choosing the parameter when tuning is performed. ııғсм method results in significant performance increase compared to other existing methods [41, 32].

The clustering algorithms are based on ıғs also suffer from initial centroid selection. In this paper, a novel algorithm is presented to obtain the melanoma regions from skin images. The proposed method identifies the initial regions using triangular fuzzy sets. The obtained regions are considered for different membership functions for IFS and the centroids are also initialized with mean values of the regions. The updating of the centroids and the membership functions of IFS are iterated until clusters are stable and exactly identify the melanoma regions. The algorithm extracts the melanoma regions effectively when compared to other existing algorithms.

The paper has different sections which explains the background in Section 2, Triangular Intutionistic Fuzzy C-Means (ҭıғсм) in Section 3, implementation and results analysis in section 4 and finally conclusions and the future scope in Section 5.

2. Background

2.1. Challenges of Skin cancer detection

Skin cancer detection is a challenging task due to numerous artefacts associated with the skin medical images.

2.1.1. Irregular shape,size and shade

Huge changes among skin lesions has complicated the detection and segmentation of skin lesions accurately. Numerous factors like lesion localization, its size, shape, skin hair, bubbles, blood vessels, uneven boundaries with fuzziness, and tone of the skin, need to be handled with pre processing for accurate segmentation.

2.1.2. Image acquisition artefacts

The artefacts related to image acquisition include rule marker, imaging frames, low contrast and illumination. Figure 1 depicts the artefacts that make skin cancer detection more complex.

2.2. Pre-Processing and post Processing

Pre-processing is preformed on the data sets in different ways. Initially the images are converted to gray scale and resize is performed as different data sets contain varied sizes of images. Here no further pre-processing is performed as intuitionistic sets are used to obtain the lesion belonging and non belonging and fuzzy boundaries based on the membership function. As part of post processing binarization,is performed on the lesion belonging region to obtain the lesion region.
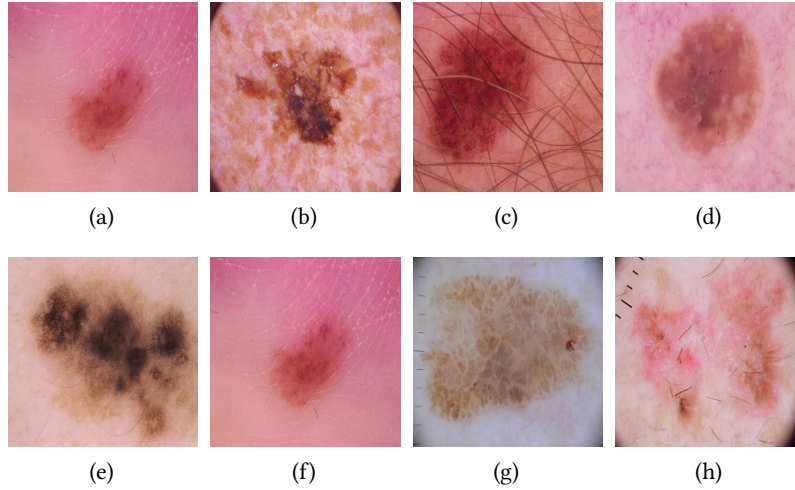
Figure 1: Images from HAM10000 data set (a)skin tone (b)irregular shape (c) hair (d) air bubble images (e)fuzzy boundaries (f) cracked skin tones (g)rule markers (h) imaging frames

2.3. Fuzzy sets and Triangular fuzzy membership function

Definition 1. The definition of fuzzy set is notated by a membership function $\mu_{\bar{a}}(e)$ where E is the universe of discourse.This function establishes a mapping between each element $e \in E$ to a real valued number in the range $[0, 1]$. This membership function reveals the grade of membership of the element e in $\mu_{\bar{a}}(e)$. As the value of the function gets closer to unity, the higher will be the membership grade.

Definition 2. The function $\mu_{\bar{a}}(e)$ for a triangular fuzzy number $\tilde{a} = (a1, a2, a3)$ is established as:

$$\mu_{\bar{a}}(e) = \begin{cases} 0 & \text{if } e < a1 \\ \frac{e-a1}{a2-a1} & \text{if } a1 < e \leq a2 \\ \frac{a3-e}{a3-a2} & \text{if } a2 < e < a3 \\ 0 & \text{Otherwise} \end{cases} \quad (1)$$

The values of the triplet $(a1, a2, a3)$ are real numbers that confines to $a1 \leq a2 \leq a3$. The value of e at the triplet element $a2$ is the most likely value of the evaluation data and it is also observed as the supreme grade of $\mu_{\bar{a}}(e)$. On the other hand, the minimum grade of e at $\mu_{\bar{a}}(e)$ is the least likely value to be evaluated from the membership function i.e., $\mu_{\bar{a}}(e) = 0$. The range of evaluation data is bounded between the constants $[a1, a3]$, which is an implication of degree of fuzziness of the evaluation data.

2.4. Intuitionistic fuzzy sets:

Generalization of fuzzy sets is characterised by membership, non-membership and hesitancy values [42]. The degree of belongingness to a cluster determines the membership and non-membership property of the elements. The dilemma of a particular pixel belonging to a specific

cluster is determined by the hesitancy. Hesitancy adds preciseness to the imperfect knowledge obtained from the fuzzy sets.

$$A = \{(e, \mu_A(e), \pi_A(e)) \mid e \in E\} \tag{2}$$

with $\gamma_A(e) = 1 - (\mu_A(e) + \pi_A(e))$ where the functions $\mu_A(e), \pi_A(e)$ indicates the degree of belongingness and non-belongingness of an element to the finite set E. The intuitionistic fuzzy index is determined by $\gamma_A(e)$, which signifies the degree of hesitation of an element. The necessary conditions to be satisfied for element $e \in E$ that is defined as IFS is given by $0 \leq \mu_A(e), \gamma_A(e), \pi_A(e) \leq 1$. The bias, noise and assignment of an element to a particular cluster is precisely represented by the three functions.

2.5. Data Sets

There are different data sets available to work with skin cancer algorithms.

PH2 [43] comprises of epiluminoscopy images which is otherwise called as dermoscopic images contains the size of 768X560 pixel values. This datasets has 200 melanocytic lesions images consisting of nevi, sensitive nevi and melanomas. This dataset also contains numerous images descriptors as well.

ISIC 2019 dataset is categorized into 8 different classes of dermoscopic images for training and testing. The datasets are available with and with out metadata containing a total 25,331 images. The Groundtruth's are also available for the standard images of lesion for testing.This dataset is originated from BCN20000, HAM10000 and MSK Datasets. [41, 44]

HAM10000 [45] as the name indicates, it contains 10,015 images for training and were categorised in to different dermatoscopic images in realm of pigmented lesions collected from varied population. They were collected, confirmed and stored through different modalities rate. [45]. They are available for the research and public use in the ISIC collection.

2.6. Pre-Processing

3. Proposed Methodology

This section mainly concentrates on the flow of segmentation performed on skin images using triangular intuitionistic fuzzy sets.

3.1. Triangular membership based fuzzy region determination

The Fuzzy functions highly impact the segmentation performance as these are necessary for producing clusters. The proposed method presents a novel approach by identifying the initial regions with the triangular membership functions which act as the input to the intutionistic fuzzy c-means. The observed image having the size $m \times n$ be notated as $E = \{e_i/e_i$ represents i^{th} pixel value in the image $\}$. In order to apply triangular membership function a, b and c values are needed. These values are calculated from the gray values associated with the peaks and valleys of the histogram of the image [46]. Figure 2 show the ISIC images and their
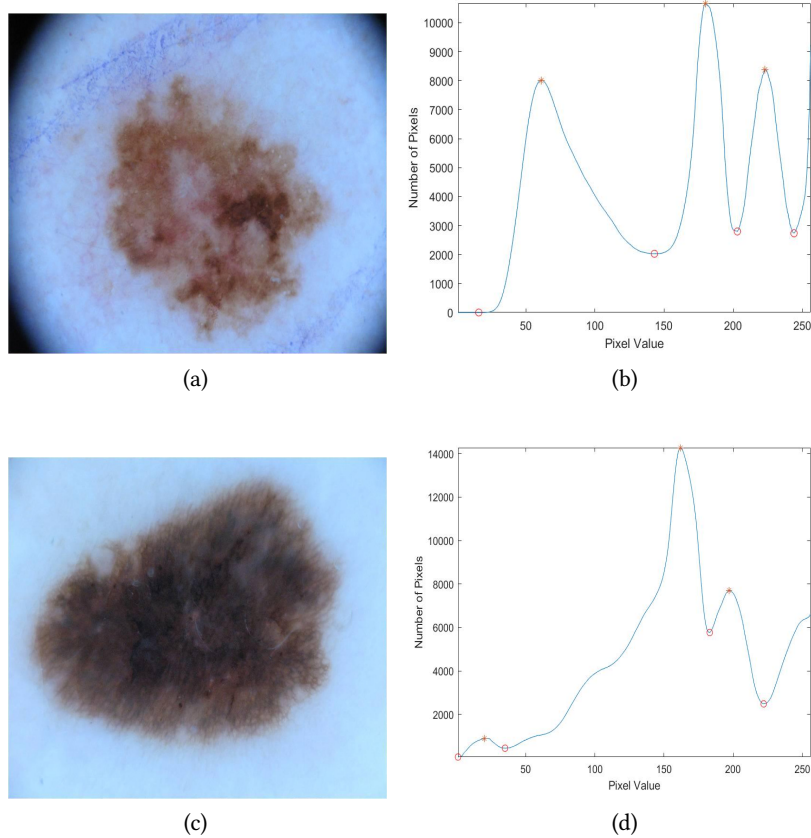
Figure 2: (a)(c) ISIC sample Images (b)(d) valleys and peaks of the images

corresponding peaks and valleys. Every sequence of valley, peak and valley will be treated as $a1, a2$ and $a3$ that will extract the membership $\mu_{\bar{a}}(e)$ for the regions using Equation 1.

The regions obtained from the triangular membership function are given as input to the intuitionistic fuzzy c-means. Figure 3 shows the regions extracted using triangular membership function.

3.2. Triangular Intuitionistic fuzzy c-means (TIFCM)

The regions obtained from the triangular membership function are used to find the centroids needed to perform intuitionistic fuzzy c-means. Many image segmentation works based on IFS are proposed in [47, 48, 32]. The image E is corelated to intuitionistic fuzzy with the below equation

$$A = \{(e_i, \mu(e_i), \pi(e_i)) \mid e_i \in E\} \tag{3}$$

In order to find $\mu(e_i), \pi(e_i)$ and $\gamma(e_i)$, membership functions, the three regions obtained with a, b, c of triangular membership function is considered as deterministic region $D(e_i), H(e_i)$ and
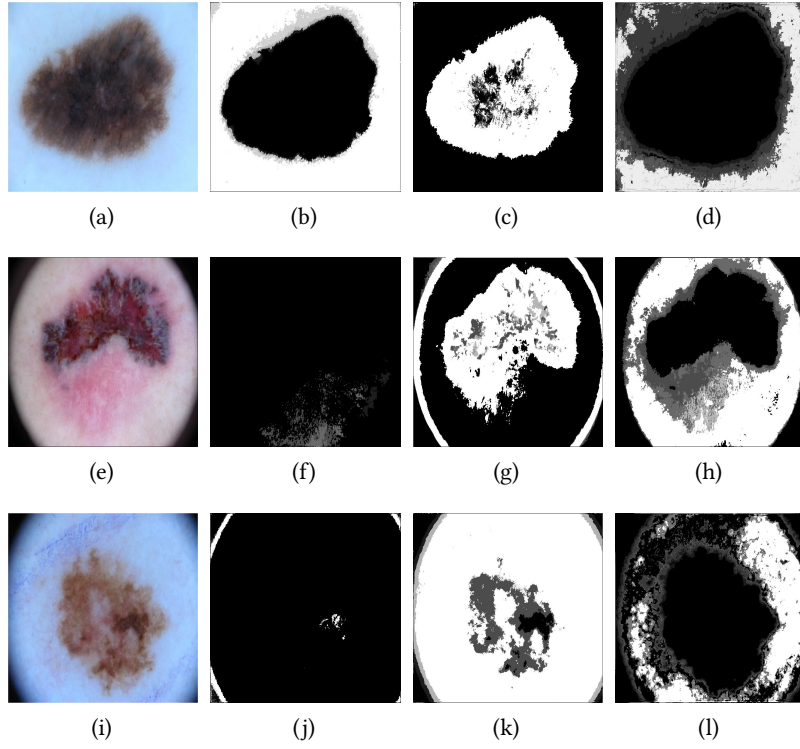
Figure 3: (a)(e)(i) Images from ISIC data set, (b)(f)(j) regions extracted for values $a1 < e_i \leq a2$, (c)(g)(k) regions extracted for values $a2 < e_i \leq a3$, (d)(h)(l)other region for values $e_i \leq a1$ and $e_i \geq a3$.

other region as indeterminacy region $I(e_i)$. Compute the mean value of every region to obtain the initial centroids C_j where $1 < j < n$ (n is the 3 for three regions).

The computation of membership value $\mu(e_i)$ is performed with the deterministic region $D(e_i)$ and the centroids with the below Eq. 4.

$$\mu(e_i) = \cfrac{1}{\displaystyle\sum_{j=1}^{n} \left(\cfrac{||D(e_i)-C_j||}{\displaystyle\sum_{c=1}^{n,c!=j}||D(e_i)-C_c||} \right)^{\frac{2}{m-1}}} \tag{4}$$

where C_j is the centroid of jth cluster (here, mean value of $(D(e_i))$ and C_c is the centroid values of regions other than j^{th} cluster (here, $H(e_i), I(e_i)$) are obtained from triangular membership function). Compute $\pi(e_i)$, and $\gamma(e_i)$ with the help of $I(e_i)$ and $H(e_i)$ by making use of Eqs.(5)-(6).

$$\pi(e_i) = \cfrac{1}{\displaystyle\sum_{j=1}^{n} \left(\cfrac{||I(e_i)-C_j||}{\displaystyle\sum_{c=1}^{n,c!=j}||I(e_i)-C_c||} \right)^{\frac{2}{m-1}}} \tag{5}$$

$$\gamma(e_i) = \cfrac{1}{\displaystyle\sum_{j=1}^{n}\left(\cfrac{||H(e_i)-C_j||}{\displaystyle\sum_{c=1}^{n,c!=j}||H(e_i)-C_c||}\right)^{\frac{2}{m-1}}} \tag{6}$$

The IFS partition matrix $\mu_{IFS}(e_i)$ and cluster centroid $C(\mu(e_i))$ are updated using the below equations.

$$\mu_{IFS}(e_i) = \mu(e_i) + \pi(e_i) + \gamma(e_i) \tag{7}$$

$$C(\mu(e_i)) = \cfrac{\displaystyle\sum_{e_i \in E}(\mu(e_i))^m(e_i)}{\displaystyle\sum_{e_i \in E}(\mu(e_i))^m} \tag{8}$$

Find the other centroids using the Equation 8 for $\pi(e_i)$ and $\gamma(e_i)$. Here, m indicates the fuzzification constant given by user. The membership function converts to be crisp and binary if the values m nears to 1 otherwise fuzzy and blurred with increased value [49]. Good segmentation results are produced for vast data with $1.5 < m < 3$ and generally 2 is considered[50, 51].

Triangular intuitionistic fuzzy c-means is also iterative similar to other clustering algorithms. It finds the three regions using Equations 4,5,6 and obtains the new centroids using Equation 8 repeatedly and stops when the clusters are stable. The stability of cluster is computed with the similarity coefficient based on the Hamming distance between the previous clusters $\mu(e_i))^l, \pi(e_i)^l$ and $\gamma(e_i)^l$ and present cluster $\mu(e_i))^{l+1}, \pi(e_i)^{l+1}$ and $\gamma(e_i)^{l+1}$. The hamming distance is given with the equation

$$\begin{aligned} sc = \sum_{i=1}^{M*N} & \mid \mu_(e_i)^l - \mu_(e_i)^{l+1} \mid \\ & + \mid \pi(e_i)^l - \pi(e_i)^{l+1} \mid \\ & + \mid \gamma(e_i)^l - \gamma(e_i)^{l+1} \mid \end{aligned} \tag{9}$$

3.3. Triangular intuitionistic fuzzy c-means clustering Algorithm (TIFCM)

The step-wise algorithm of Triangular intuitionistic fuzzy is listed below.

Algorithm 1 Segmentation algorithm for images with generalized triangular intuitionistic fuzzy sets
---
INPUT: TIFCM image E and ϵ exit criteria with 0.01.

OUTPUT: n number of clusters to be generated for representing the regions of skin image contain a, b, c values for each regions using method defined by [46]

1 Obtain a,b,c values for each regions using method defined by [46].

2 Obtain the three regions $D(e_i), H(e_i)$ and $I(e_i)$ as per Eq. 1 .

3 Find the cluster centroids C_j from the regions by finding the mean value of the region.

4 while true

4.1 for every j in n clusters and every e_i in E obtain three intuitionistic membership function values using Eq. 4-6

4.2 Update the partition matrix $\mu_{IFS}(e_i)$ and the cluster centroid C_j using Eq. 7 and Eq. 8.

4.3 Estimate the similarity coefficient(sc) using Eq.9

4.4 If $sc \leq \epsilon$ then break else compute $\mu_{IFS}(e_i)^l = \mu_{IFS}(e_i)^{l+1}$ and repeat 4.

5 with stable $\mu_{(e_i)}$, $\gamma_{(e_i)}$ and $\pi_{(e_i)}$ obtain n clusters.
---

4. Implementation and Experimental Results

4.1. Experimental Setup

In order to find the efficacy of the proposed algorithm TIFCMM, The ISIC 2016, HAM10000 2019 data set [44] and PH2[43] data set is used. The data set contains the skin images with diagnostic, clinical, technical and database attributes based images. The proposed TIFCM algorithm is worked out with MATLAB software on i5 processor. The total number of clusters n is assigned as 3 in the proposed algorithm to determine the three regions regions. The centroid values are initialised through the triangular membership functions. The difference between the subsequent clusters is fixed as the exit criteria, which is 0.01.

As part of pre-processing the images are resized to 512×640 as the image sizes vary for ISIC, PH2 HAM10000 data sets. In post processing of the proposed algorithm, the deterministic final region is converted to black and white in order to compare with the ground truths.

The segmentation results of the TIFCM algorithm on various skin images is shown in Fig. 4. Column 1shows the Original images of ISIC data sets. The images (a)ISIC_0000000,(e) ISIC_0000008 (i)ISIC_0000049 (m) ISIC_0000008 (q) ISIC_0000002 (u) ISIC_0000043 are shown in Column 1 and are used to extract malignant region using proposed TIFCM. Column 2 shows the Deterministic region depicting cancer region, Column 3 depicting Indeterminacy regions and Column 4 showing the Hesitance regions extracted from the stable clusters of TIFCM. Further, in Fig. 5 the segmentation results of images ISIC0034329, ISIC0034332, ISCI0034337 and ISIC0034343 of ISIC 2019 data set are presented. The subjective analysis show that the lesion was extracted efficiently using the proposed method.

Fig. 6 exhibits the results of TIFCM algorithm for different images like malignant melanoma, melanoma, benign melanoma, common nevus, a typical nevus image that are commonly identified skin diseases of PH2 data set. The lesion detection of these images are compared with their ground truths [5]. The results showed that the proposed algorithm performs very well when
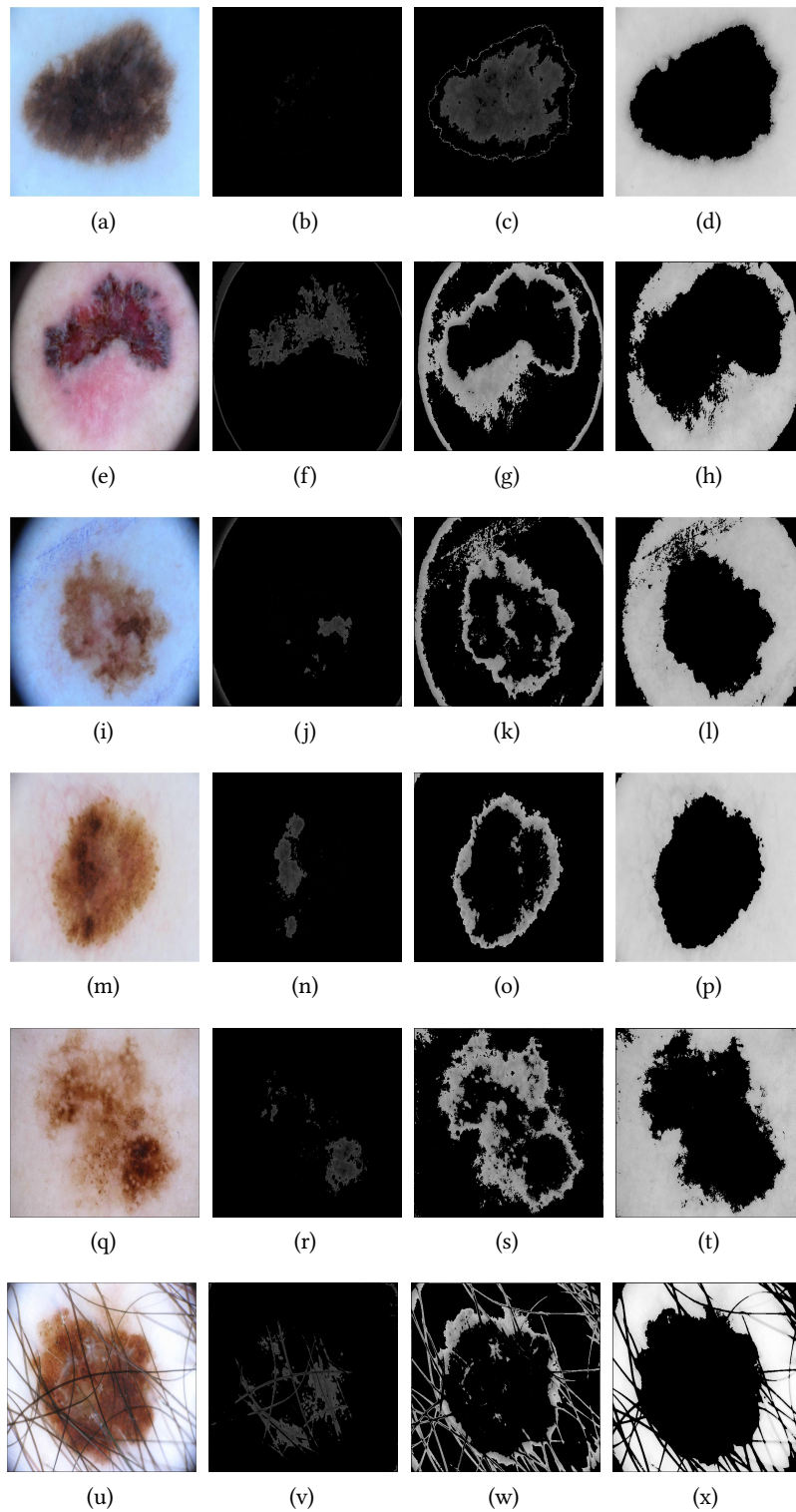
Figure 4: Segmentation results of proposed algorithm TIFCM for different images of ISIC data set. (Column 1) Original images of ISIC data sets, (Column 2) Deterministic region depicting cancer region, (Column 3) Indeterminacy regions (Column 4) Hesitance regions.

Figure 5: Segmentation results of proposed algorithm TIFCM for ISIC_0034329, ISIC_0034332, ISCI_0034337 and ISIC_0034343 of ISIC 2019 data set. (Column 1) Original images of ISIC data sets, (Column 2) Deterministic region depicting cancer region, (Column 3) Indeterminacy regions (Column 4) Hesitance regions.
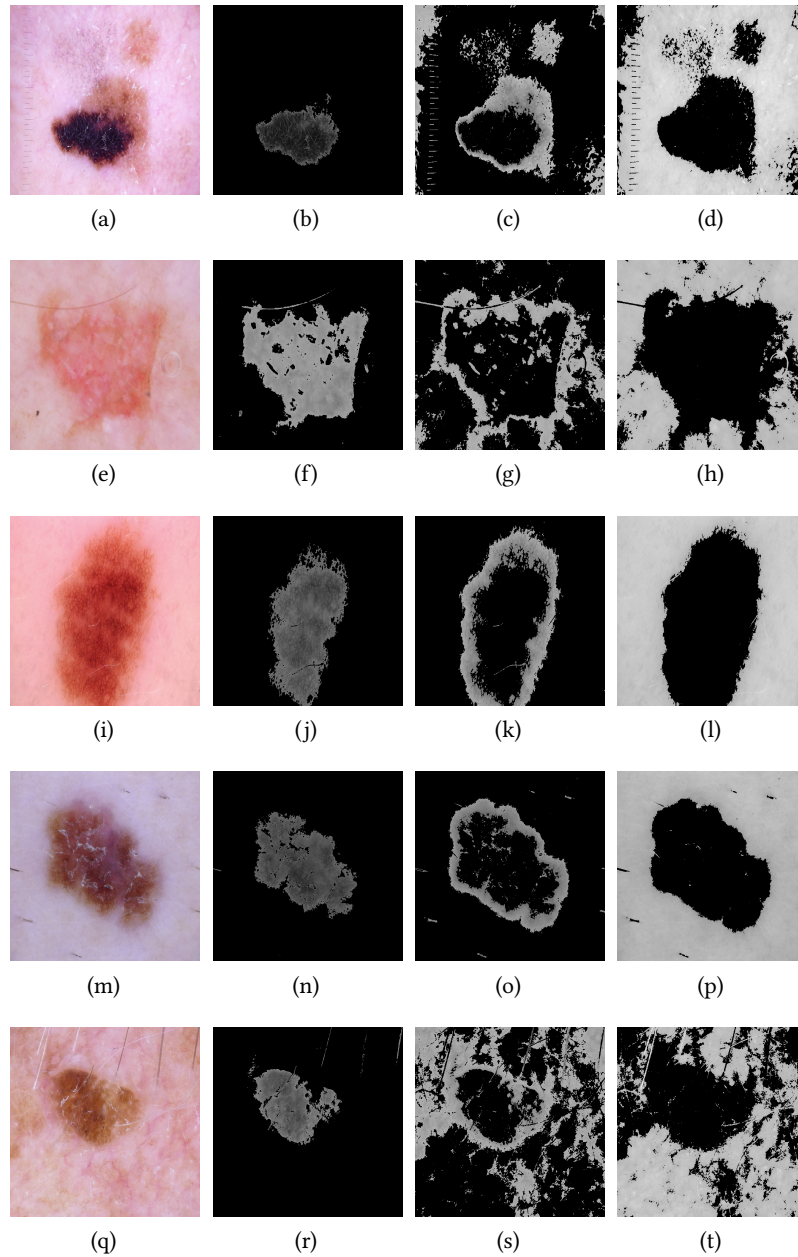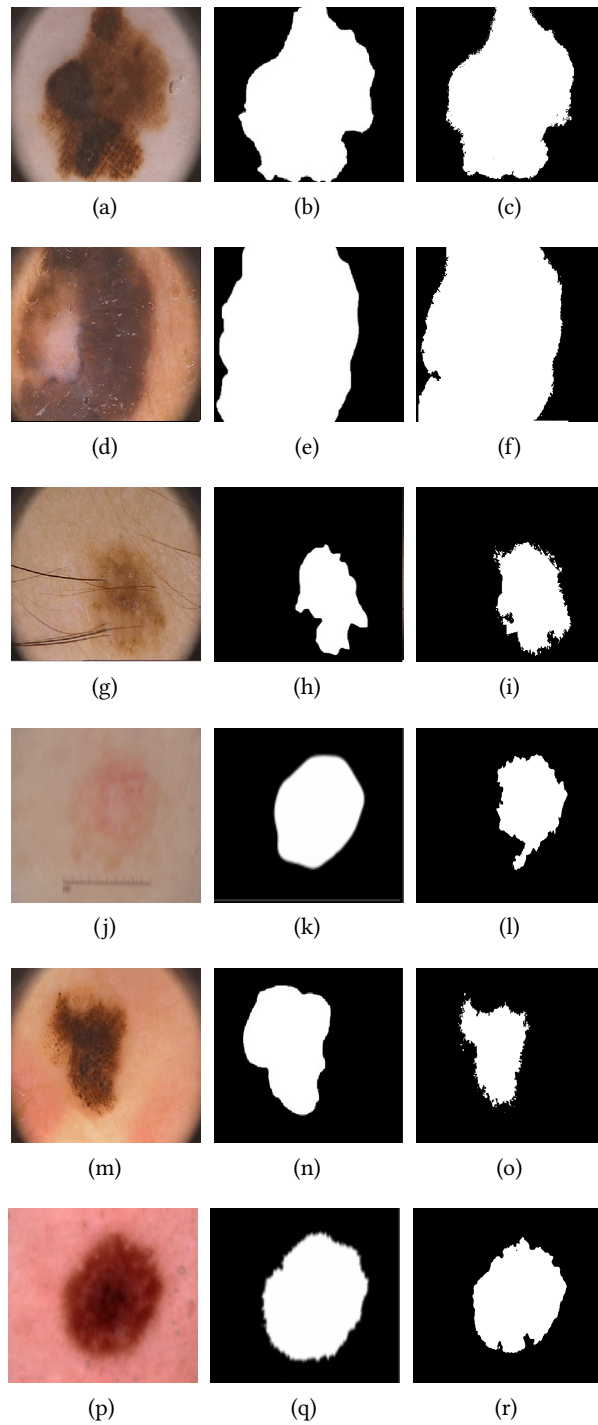
Figure 6: Lesion segmentation of different PH2 data set images.(Row 1) (a) Malignant melanomas image IMD063, (b) Ground Truth(GT), (c) extracted using TIFCM. (Row 2) (d) Melanoma image IMD058,(e) GT of IMD058, (f) extracted using TIFCM. (Row 3) (g) A typical Nevus image IMD048, (h) GT of IMD048, (i)extracted using TIFCM .(Row 4) (j)Common Nevus image ISIC_0012253, (k) GT of (j), (l) extracted using TIFCM.(row 5) (m) Benign melanoma image IMD075, (n) GT of IMD075, (o) extracted using TIFCM. (row 6) (p) Benign melanoma image ISIC_0000125, (q) GT of (p), (r) extracted using TIFCM.

compared to other algorithms. The comparative analysis of the proposed algorithms with other state of art techniques namely KM [52], FCM [50], RFCM [53], and GRIFCM [32] is given in Fig 7 . The detailed analysis with other segmentation algorithms reveals that the proposed algorithm gives improved cancer region segmentation.

4.2. Quantitative Analysis

The segmentation results are analysed quantitatively using the performance measures namely, segmentation accuracy (SA), jaccards coefficient (JC) and Dice coefficient (DC) .

$$\text{Jaccard coefficient} = \frac{E1 \bigcap E2}{E1 \bigcup E2} \tag{10}$$

$$\text{Dice coefficient} = \frac{2 \mid E1 \bigcap E2 \mid}{\mid E1 \mid + \mid E2 \mid} \tag{11}$$

where $E1$ is the ground truth image. $E2$ is the resultant segmented image,

$$\text{Segmentation Accuracy} = \frac{TP + FN}{TP + FN + TN + FN} \tag{12}$$

where,

1. True positive (TP): Ratio of sum of true pixels in the E2 detected in E1.
2. True negative (TN): Ratio of sum of true pixels in the E2 falsely segmented as negative in E1.
3. False positive (FP): Ratio of sum of false pixels in E2 falsely segmented as positive in E1.
4. False negative (FN): Ratio of sum of false pixels in E2 detected as negative in E1.

Table 1
Comparisons of performance measures for the images in Figure 3.

Images	SA	JC	DC	Precision	Sensitivity	Specificity
Malignant Melanoma	0.9059	0.8799	0.8438	0.8797	0.9206	0.8935
Melanoma	0.9308	0.9341	0.7939	0.9396	0.9530	0.8915
A typical Nevus	0.9185	0.7424	0.8071	0.7468	0.7868	0.9585
Common Nevus	0.8719	0.8323	0.8123	0.8623	0.9880	0.8639
Benign Melanoma	0.8689	0.7921	0.8528	0.8121	0.9853	0.8520

The SA, JC, DC, precision, specificity and sensitivity measures are given in Table 1. These performance measures are calculated for different skin disease, namely, malignant melanoma, melanoma, benign melanoma, common nevus, typical nevus images of ISIC data set images. The results proved that the proposed algorithms have efficiently extracted the lesion of an cancerous tissues. The average JC value of 0.85, SA of 0.90 is achieved for with the proposed TIFCM. The quality of segmentation can be assessed by observing the segmentation JC value with 0.8 or above indicating the visual "correctness". It is observed that for 100 images from ISIC 2019 the observant agreement for JC value is considered as 0.786[44]. It is observed that, the fall in

Table 2

Comparisons of performance measures for different segmentation Algorithms.

Algorithm	SA	JC	Sensitivity	Specificity	DC
Yolo et al. [26]	0.929	0.795	0.836	0.940	0.881
Yuan et al. [6]	0.930	0.765	0.825	0.975	0.849
Li et al.[27]	0.932	0.7620	0.820	0.978	0.847
Lin et al.[28]	-	0.620	-	-	0.770
FCM [54]	0.884	0.665	0.869	0.923	0.884
TIFCM	0.905	0.856	0.952	0.862	0.830

Table 3

Execution time comparison for different Algorithms

KM	FCM	RFCM	GRIFCM	TIFCM
38.5 ± 2.3	35.8 ± 2.5	32.4 ± 2.1	20.5 ± 3.2	16.56 ± 2.5

JC value below 0.7, the "correctness" of the segmentation can be debated. With the proposed method,78 out of 100 images fell above JC of 0.7, 10 images fell at or below 0.7, rest images fell below 0.6.

In order to depict the efficiency and robustness of the proposed TIFCM method, a comparison with the latest methods in the literature, are shown in Table 2. The methods used in the comparison are executed on ISIC 2017 challenge and are ranked based on the Jaccards coefficient. It is clear from the table that the JC values produced with the proposed method has an marginal increment over other lesion segmentation algorithms.Also, the improved sensitivity values are observed with the proposed method. In contrast, the deep learning methods have exhibited high segmentation accuracy and specificity. The proposed method dice coefficients are inline with the results of the deep learning methods.

The efficacy of the proposed method is also compared with the method FCM classification of pixels with histogram thresholds [54]. The SA, JC and sensitivity values are significantly improved with the proposed methods while the specificity and DC values are less with the proposed method.

5. Conclusion

Computer aided detection of malignant melanoma skin cancer with the use of skin images has tremendously assisted the clinicians. Due to numerous factors like artifacts in skin images, non homogeneous intensity and low contrast images skin cancer detection increased complexity. In this paper, we present a novel TIFCM algorithm for skin image segmentation. Triangular membership function is used to extract the initial regions and centroids. This avoids the initial selection of centroids which is the drawback of every clustering algorithm. The triangular membership based centroids and regions assist in faster stability of clusters reducing the execution time. The regions extracted are used as initial inputs to calculate the membership functions of the intuitionistic fuzzy c-means that effectively handles the uncertainty in the skin images.

Declarations

- Funding-Not Applicable
- Conflict of interest/Competing interests- Not Applicable

References

[1] R. B. Oliveira, E. Mercedes Filho, Z. Ma, J. P. Papa, A. S. Pereira, J. M. R. Tavares, Computational methods for the image segmentation of pigmented skin lesions: a review, Computer methods and programs in biomedicine 131 (2016) 127–141.

[2] D. Koundal, B. Sharma, Advanced neutrosophic set-based ultrasound image analysis, in: Neutrosophic set in medical image analysis, Elsevier, 2019, pp. 51–73.

[3] M. A. Al-Masni, M. A. Al-Antari, M.-T. Choi, S.-M. Han, T.-S. Kim, Skin lesion segmentation in dermoscopy images via deep full resolution convolutional networks, Computer methods and programs in biomedicine 162 (2018) 221–231.

[4] O. O. Olugbara, T. B. Taiwo, D. Heukelman, Segmentation of melanoma skin lesion using perceptual color difference saliency with morphological analysis, Mathematical Problems in Engineering 2018 (2018).

[5] A. Pennisi, D. D. Bloisi, D. Nardi, A. R. Giampetruzzi, C. Mondino, A. Facchiano, Skin lesion image segmentation using delaunay triangulation for melanoma detection, Computerized Medical Imaging and Graphics 52 (2016) 89–103.

[6] Y. Yuan, Automatic skin lesion segmentation with fully convolutional-deconvolutional networks, arXiv preprint arXiv:1703.05165 (2017).

[7] K. Korotkov, R. Garcia, Computerized analysis of pigmented skin lesions: a review, Artificial intelligence in medicine 56 (2012) 69–90.

[8] N. Otsu, A threshold selection method from gray-level histograms, IEEE transactions on systems, man, and cybernetics 9 (1979) 62–66.

[9] M. E. Yüksel, M. Borlu, Accurate segmentation of dermoscopic images by image thresholding based on type-2 fuzzy logic, IEEE Transactions on Fuzzy Systems 17 (2009) 976–982.

[10] C. Barata, M. Ruela, M. Francisco, T. Mendonça, J. S. Marques, Two systems for the detection of melanomas in dermoscopy images using texture and color features, IEEE Systems Journal 8 (2013) 965–979.

[11] H. Zhou, G. Schaefer, A. H. Sadka, M. E. Celebi, Anisotropic mean shift based fuzzy c-means segmentation of dermoscopy images, IEEE Journal of Selected Topics in Signal Processing 3 (2009) 26–34.

[12] H. Castillejos, V. Ponomaryov, L. Nino-de Rivera, V. Golikov, Wavelet transform fuzzy algorithms for dermoscopic image segmentation, Computational and mathematical methods in medicine 2012 (2012).

[13] G. Castiello, G. Castellano, A. M. Fanelli, Neuro-fuzzy analysis of dermatological images, in: 2004 IEEE International Joint Conference on Neural Networks (IEEE Cat. No. 04CH37541), volume 4, IEEE, 2004, pp. 3247–3252.

[14] J. Maeda, A. Kawano, S. Yamauchi, Y. Suzuki, A. Marçal, T. Mendonça, Perceptual image segmentation using fuzzy-based hierarchical algorithm and its application to dermoscopy

images, in: 2008 IEEE Conference on Soft Computing in Industrial Applications, IEEE, 2008, pp. 66–71.

[15] J. L. G. Arroyo, B. Garcia-Zapirain, Segmentation of skin lesions based on fuzzy classification of pixels and histogram thresholding, CoRR abs/1703.03888 (2017). URL: http://arxiv.org/abs/1703.03888. arXiv:1703.03888.

[16] L. Ma, R. C. Staunton, Analysis of the contour structural irregularity of skin lesions using wavelet decomposition, Pattern recognition 46 (2013) 98–106.

[17] M. E. Celebi, H. Iyatomi, G. Schaefer, W. V. Stoecker, Lesion border detection in dermoscopy images, Computerized medical imaging and graphics 33 (2009) 148–153.

[18] B. Erkol, R. H. Moss, R. Joe Stanley, W. V. Stoecker, E. Hvatum, Automatic lesion boundary detection in dermoscopy images using gradient vector flow snakes, Skin Research and Technology 11 (2005) 17–26.

[19] F. Riaz, S. Naeem, R. Nawaz, M. Coimbra, Active contours based segmentation and lesion periphery analysis for characterization of skin lesions in dermoscopy images, IEEE journal of biomedical and health informatics 23 (2018) 489–500.

[20] V. Rajinikanth, N. Madhavaraja, S. C. Satapathy, S. L. Fernandes, Otsu's multi-thresholding and active contour snake model to segment dermoscopy images, Journal of Medical Imaging and Health Informatics 7 (2017) 1837–1840.

[21] F. F. X. Vasconcelos, A. G. Medeiros, S. A. Peixoto, P. P. Rebouças Filho, Automatic skin lesions segmentation based on a new morphological approach via geodesic active contour, Cognitive Systems Research 55 (2019) 44–59.

[22] T. J. Brinker, A. Hekler, J. S. Utikal, N. Grabe, D. Schadendorf, J. Klode, C. Berking, T. Steeb, A. H. Enk, C. von Kalle, Skin cancer classification using convolutional neural networks: systematic review, Journal of medical Internet research 20 (2018) e11936.

[23] N. N. Sultana, N. B. Puhan, Recent deep learning methods for melanoma detection: a review, in: International Conference on Mathematics and Computing, Springer, 2018, pp. 118–132.

[24] A. Marka, J. B. Carter, E. Toto, S. Hassanpour, Automated detection of nonmelanoma skin cancer using digital images: a systematic review, BMC medical imaging 19 (2019) 21.

[25] K. Munir, H. Elahi, A. Ayub, F. Frezza, A. Rizzi, Cancer diagnosis using deep learning: A bibliographic review, Cancers 11 (2019) 1235.

[26] H. M. Ünver, E. Ayan, Skin lesion segmentation in dermoscopic images with combination of yolo and grabcut algorithm, Diagnostics 9 (2019) 72.

[27] Y. Li, L. Shen, Skin lesion analysis towards melanoma detection using deep learning network, Sensors 18 (2018) 556.

[28] B. S. Lin, K. Michael, S. Kalra, H. R. Tizhoosh, Skin lesion segmentation: U-nets versus clustering, in: 2017 IEEE Symposium Series on Computational Intelligence (SSCI), IEEE, 2017, pp. 1–7.

[29] Adrian I. Ban and Delia A. Tuse, Trapezoidal/triangular intuitionistic fuzzy numbers versus interval-valued trapezoidal/triangular fuzzy numbers and applications to multicriteria decision making methods, Notes on Intuitionistic Fuzzy Sets 20 (2014) 43–51.

[30] T. Aribarg, S. Supratid, C. Lursinsap, Optimizing the modified fuzzy ant-miner for efficient medical diagnosis, Applied Intelligence 37 (2012) 357–376. doi:10.1007/s10489-011-0332-x.

[31] Y. K. Dubey, M. M. Mushrif, K. Mitra, Segmentation of brain mr images using rough set based intuitionistic fuzzy clustering, Biocybernetics and Biomedical Engineering 36 (2016) 413–426.

[32] A. Namburu, S. K. Samayamantula, S. R. Edara, Generalised rough intuitionistic fuzzy c-means for magnetic resonance brain image segmentation, IET Image Processing 11 (2017) 777–785.

[33] T. Chaira, A rank ordered filter for medical image edge enhancement and detection using intuitionistic fuzzy set, Applied Soft Computing Journal 12 (2012) 1259–1266. URL: http://dx.doi.org/10.1016/j.asoc.2011.12.011. doi:10.1016/j.asoc.2011.12.011.

[34] H. Huang, F. Meng, S. Zhou, F. Jiang, G. Manogaran, Brain Image Segmentation Based on FCM Clustering Algorithm and Rough Set, IEEE Access 7 (2019) 12386–12396. doi:10.1109/ACCESS.2019.2893063.

[35] R.UmaRani, P.Amsini, Triangular Intuitionistic Fuzzy Set for Nuclei Segmentation in Digital Cancer Pathology, IOSR Journal of Engineering (2018).

[36] S. P. Mondal, A. Goswami, S. Kumar De, Nonlinear Triangular Intuitionistic Fuzzy Number and Its Application in Linear Integral Equation, Advances in Fuzzy Systems 2019 (2019) 1–14. doi:10.1155/2019/4142382.

[37] a.K. Shaw, T. Roy, Trapezoidal intuitionistic fuzzy number with some arithmetic operations and its application on reliability evaluation, International Journal of Mathematics in Operational Research 5 (2012) 55. doi:10.1504/ijmor.2013.050512.

[38] D. F. Li, A ratio ranking method of triangular intuitionistic fuzzy numbers and its application to MADM problems, Computers and Mathematics with Applications 60 (2010) $1557 - -1570$.

[39] L. V. Tilson, P. S. Excell, R. J. Green, A generalisation of the fuzzy c-means clustering algorithm, in: International Geoscience and Remote Sensing Symposium, 'Remote Sensing: Moving Toward the 21st Century'., volume 3, 1988, pp. 1783–1784. doi:10.1109/IGARSS.1988.569600.

[40] H. Verma, R. K. Agrawal, A. Sharan, An improved intuitionistic fuzzy c-means clustering algorithm incorporating local information for brain image segmentation, Applied Soft Computing Journal 46 (2016). doi:10.1016/j.asoc.2015.12.022.

[41] N. C. Codella, D. Gutman, M. E. Celebi, B. Helba, M. a. Marchetti, S. W. Dusza, A. Kalloo, K. Liopyris, N. Mishra, H. Kittler, A. Halpern, Skin lesion analysis toward melanoma detection: A challenge at the 2017 International symposium on biomedical imaging (ISBI), hosted by the international skin imaging collaboration (ISIC), Proceedings - International Symposium on Biomedical Imaging 2018-April (2018) 168–172. doi:10.1109/ISBI.2018.8363547.

[42] K. T. Atanassov, Intuitionistic fuzzy sets, Fuzzy sets. Syst 20 (1986) 87–96.

[43] T. Mendonca, M. Celebi, T. Mendonca, J. Marques, Ph2: A public database for the analysis of dermoscopic images, Dermoscopy image analysis (2015).

[44] N. C. Codella, D. Gutman, M. E. Celebi, B. Helba, M. A. Marchetti, S. W. Dusza, A. Kalloo, K. Liopyris, N. Mishra, H. Kittler, et al., Skin lesion analysis toward melanoma detection: A challenge at the 2017 international symposium on biomedical imaging (isbi), hosted by the international skin imaging collaboration (isic), in: 2018 IEEE 15th International Symposium on Biomedical Imaging (ISBI 2018), IEEE, 2018, pp. 168–172.

[45] P. Tschandl, C. Rosendahl, H. Kittler, The ham10000 dataset, a large collection of multi-source dermatoscopic images of common pigmented skin lesions, Scientific data 5 (2018) 1–9.

[46] V. D. Silva, Finding dominant peaks and valleys of an image histogram, 2020. URL: https://www.mathworks.com/matlabcentral/fileexchange/31570-finding-dominant-peaks-and-valleys-of-an-image-histogram.

[47] T. Chaira, A rank ordered filter for medical image edge enhancement and detection using intuitionistic fuzzy set, Appl. Soft Comput. 12 (2012) 1259–1266.

[48] H. Verma, R. Agrawal, A. Sharan, An improved intuitionistic fuzzy c-means clustering algorithm incorporating local information for brain image segmentation, Appl. Soft Comput. 46 (2015) 543—-557.

[49] D. L. Pham, Spatial models for fuzzy clustering, Comput. Vis. Image Underst. 84 (2001) 285–297.

[50] J. C. Bezdek, R. Ehrlich, W. Full, Fcm: The fuzzy c-means clustering algorithm, Comput. Geosci. 10 (1984) 191–203.

[51] A. Namburu, S. kumar Samay, S. R. Edara, Soft fuzzy rough set-based mr brain image segmentation, Applied Soft Computing 54 (2017) 456–466.

[52] J. T. Tou, R. C. Gonzalez, Pattern recognition, Reading, Addison-Wesley, MA (1974).

[53] P. Maji, S. K. Pal, Rfcm: a hybrid clustering algorithm using rough and fuzzy sets, Fund. Inform. 80 (2007) 475–496.

[54] J. L. Garcia-Arroyo, B. Garcia-Zapirain, Segmentation of skin lesions in dermoscopy images using fuzzy classification of pixels and histogram thresholding, Computer methods and programs in biomedicine 168 (2019) 11–19.
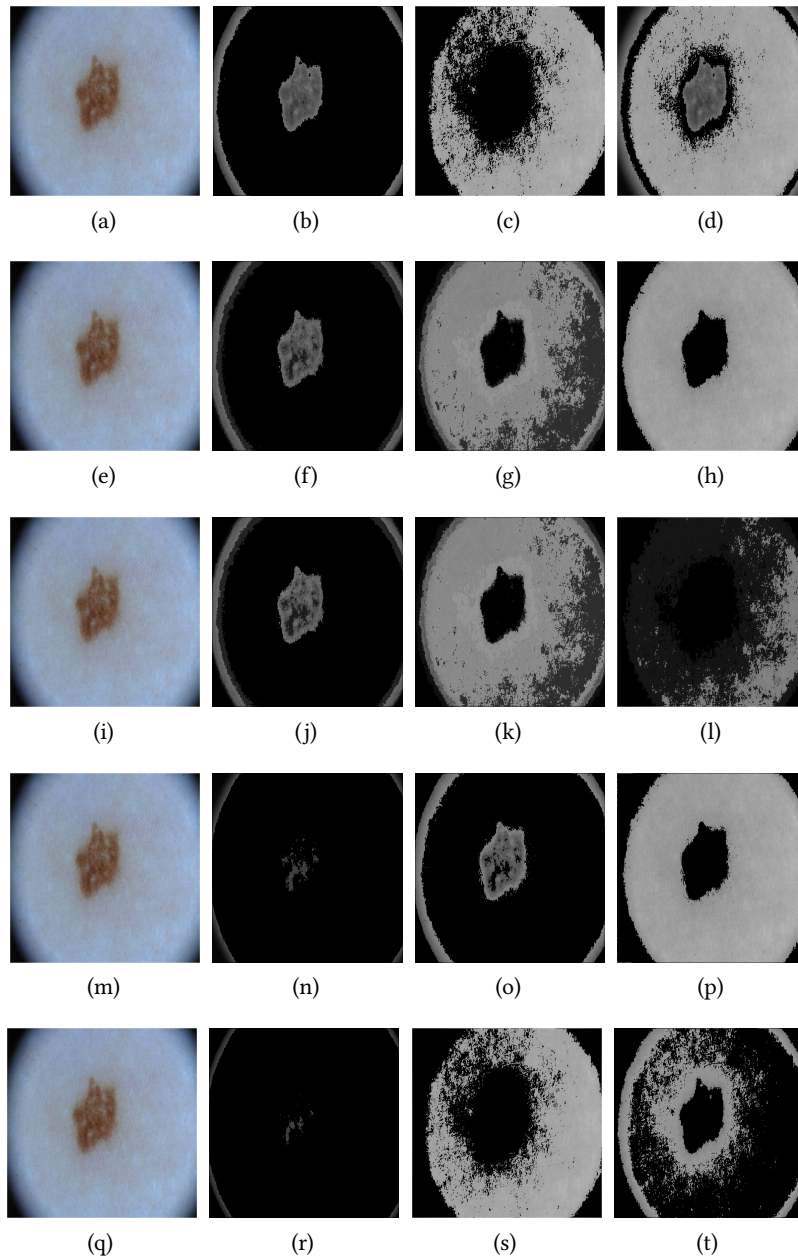
Figure 7: Comparison of Algorithms applied to ISIC_0000006 for Benign nevus detection (Row 1) Sementation with KM, (Row 2) Sementation with FCM, (Row 3) Sementation with RFCM, (Row 4) Sementation with GRIFCM, (Row 5) Sementation with TIFCM.